Supporting Information

Precise Diameter Control Derived Intermetallic PtNiCo Nanowires: A Simple Two-Step Synthesis and *Operando* XAS Insight

Kuowei Liao[1], Weijie Cao[1], Mukesh Kumar[1], Neha Thakur[1], Mitsuhiro Matsumoto[2], Toshiki Watanabe[1], Masashi Matsumoto[2, 3], Hideto Imai[2, 3], Tomoya Uruga[2], Takuma Kaneko[2], Ryota Sato[4], Toshiharu Teranishi[4], Yoshiharu Uchimoto[1, 2]*

1 Graduate School of Human and Environmental Studies, Kyoto University, Yoshida Nihonmatsu-cho, Sakyo-ku, Kyoto 606-8501, Japan
2 Office of Institutional Advancement and Communications, Kyoto University, Yoshida Honmachi, Kyoto 606-8501, Japan
3 Fuel Cell Cutting-Edge Research Center Technology Research Association, Tokyo 135-0064, Japan
4 Institute for Chemical Research, Kyoto University, Uji, Kyoto 611-0011, Japan

[*]*Corresponding author: kumar.mukesh.5x@kyoto-u.ac.jp*

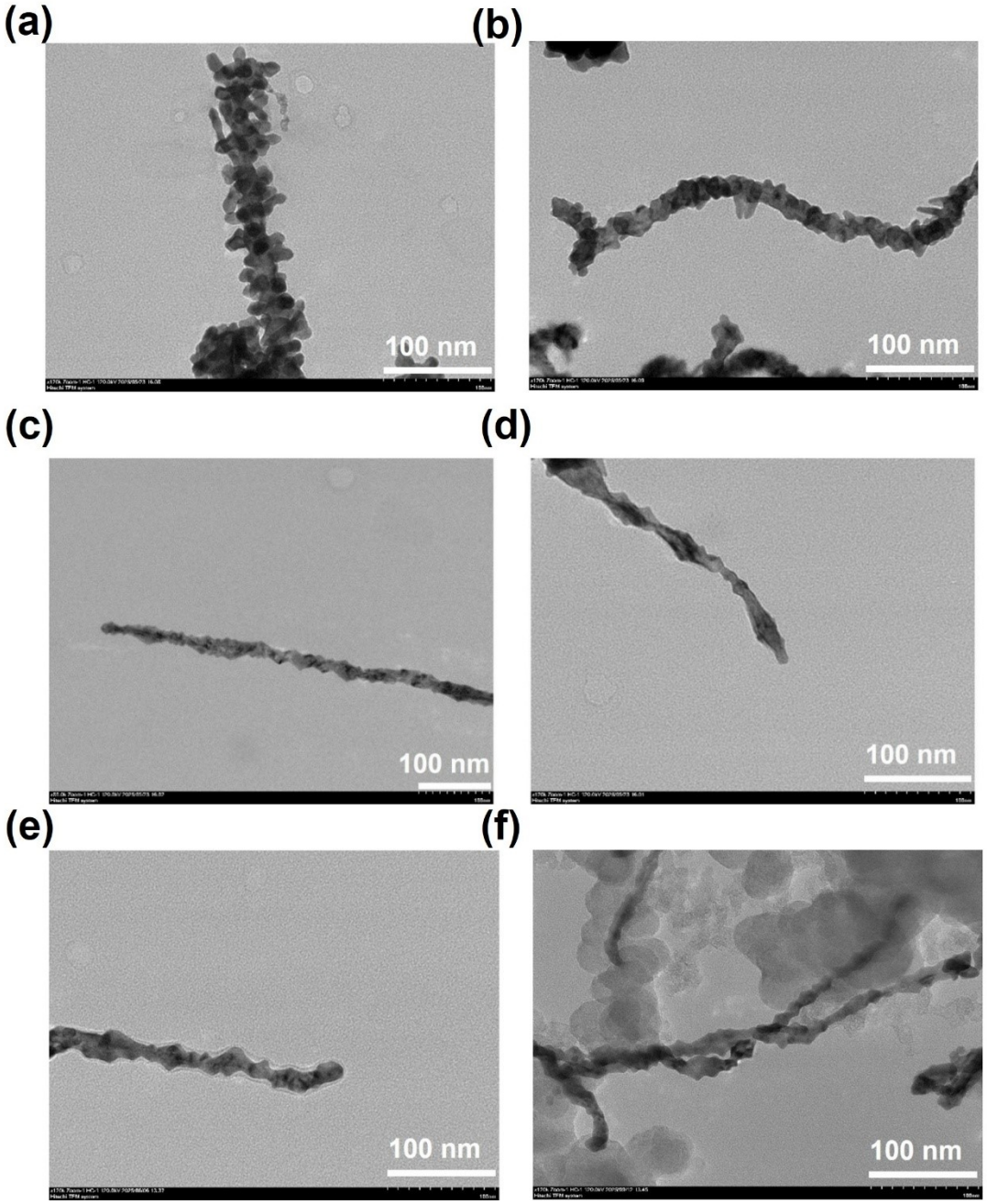

Figure S1 TEM image of D-PtNiCo-NW/C-15nm with (a,b) half amount of CTAC, (c,d) double amount of CTAC and (e,f) optimized amount of CTAC.

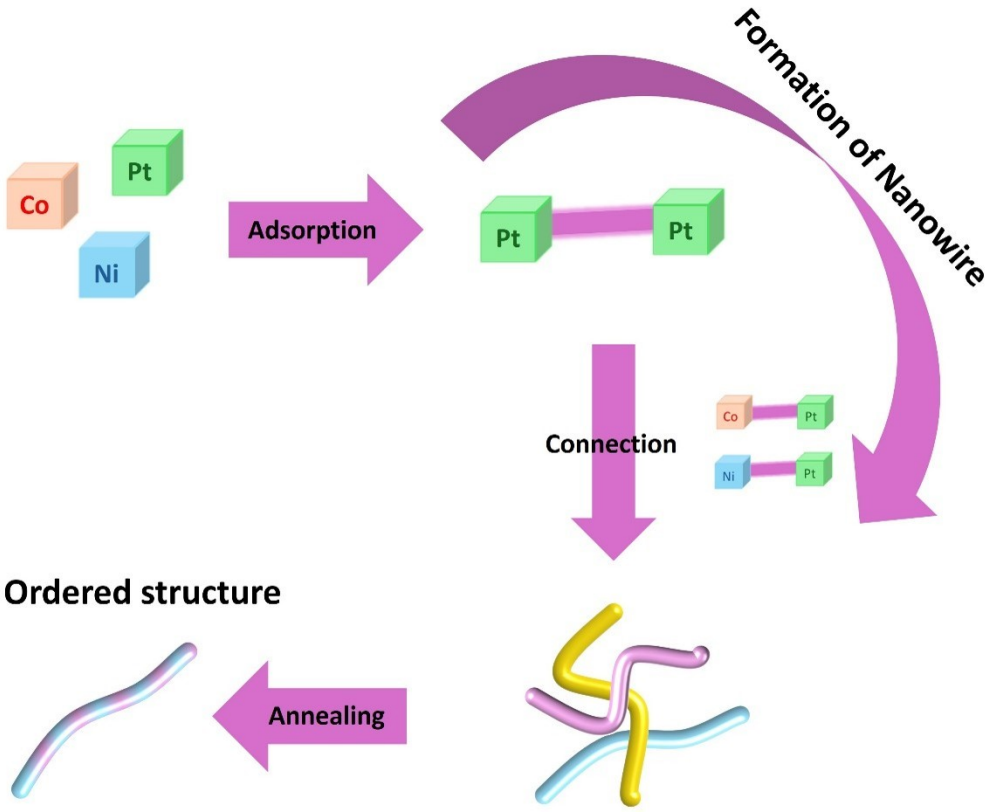

Figure S2 Proposed formation and growth PtNiCo NWs.

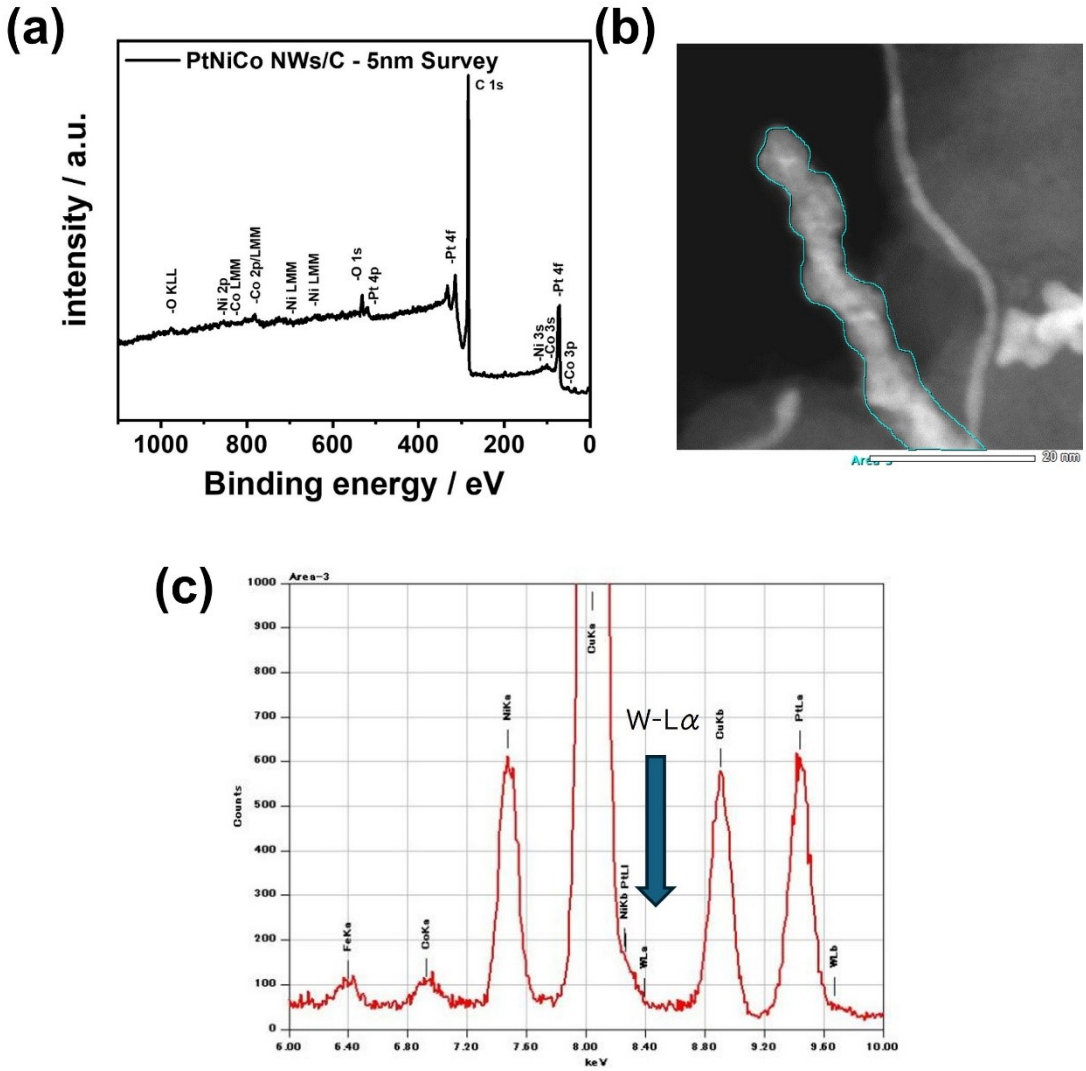

Figure S3 (a) XPS survey spectra of PtNiCo-NW/C-5nm. (b)STEM-HAADF of PtNiCo-NW/C - 5nm. (c)EDS elemental mapping of circled area in (b)

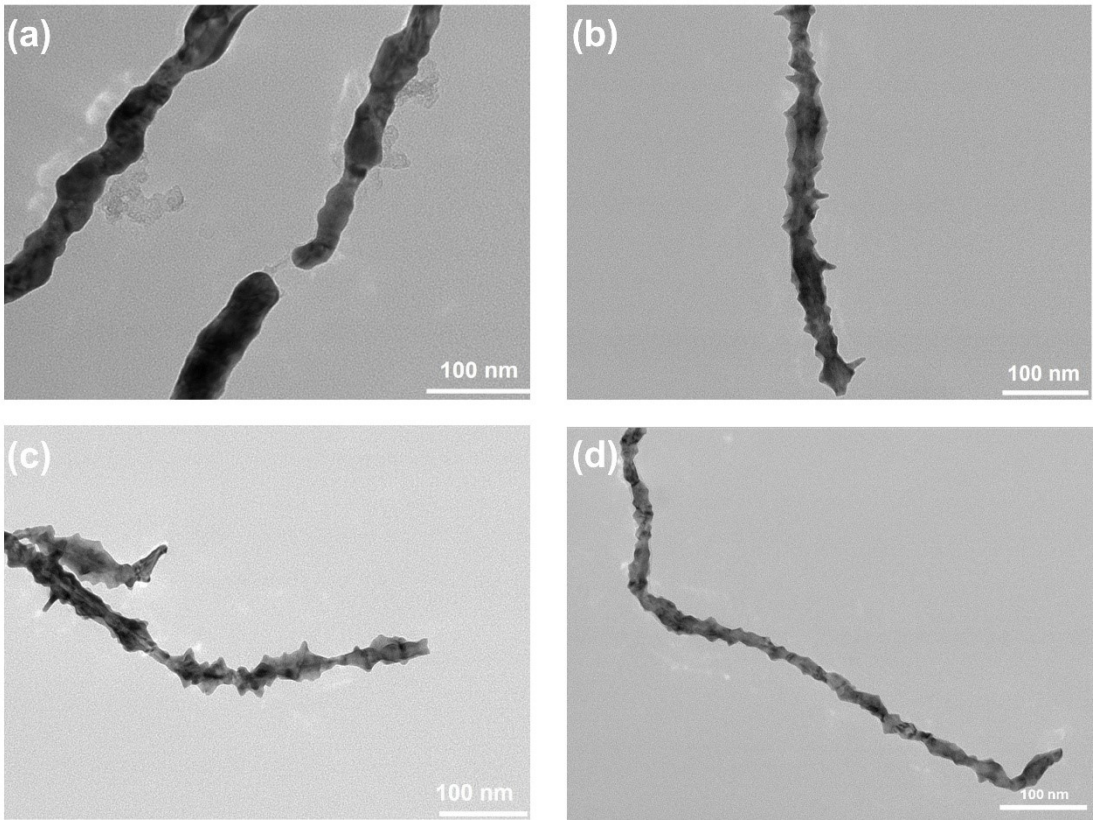

Figure S4 TEM image of PtNiCo-NW synthesized at heating ramp of (a) 3 ^{o}C/min , (b) 6 ^{o}C/min, (c)12 ^{o}C/min and (d) with pre-heated furnace,

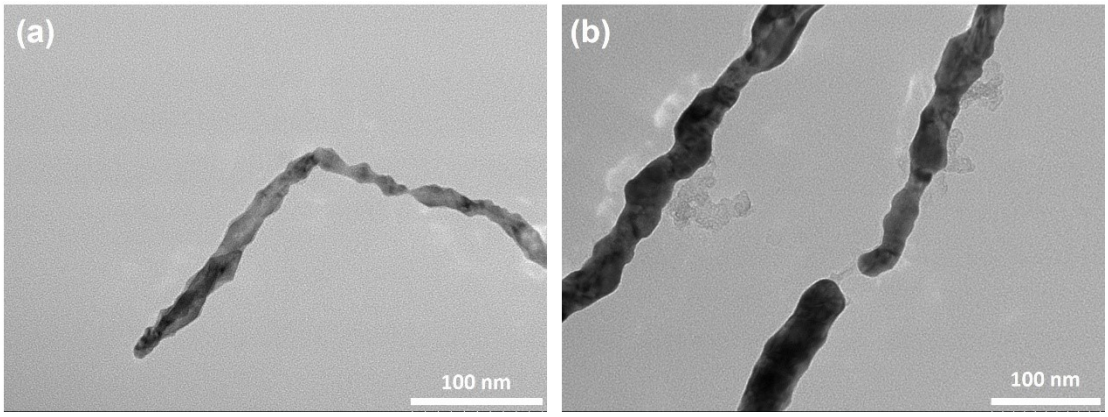

Figure S5. TEM image of (a) I-PtNiCo-NW/C-15nm catalyst. (b) I-PtNiCo-NW/C-30nm catalysts.

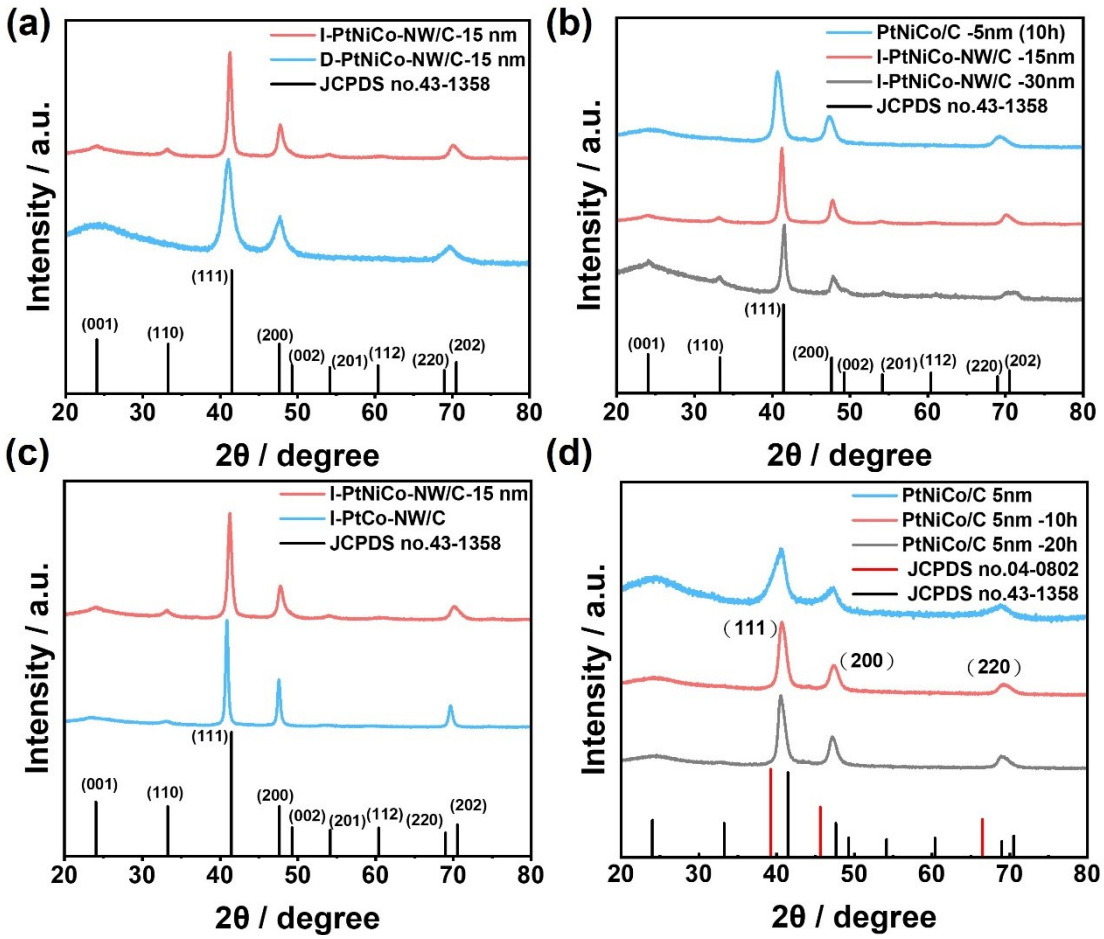

Figure S6. Powder X-ray diffraction (PXRD) patterns of (a) Disordered (D-PtNiCo-NW/C-15 nm) and intermetallic (I-PtNiCo-NW/C-15 nm) PtNiCo nanowires. (b) Intermetallic PtNiCo-NW/C with different nanowire diameters (5 nm, 15 nm, and 30 nm) after annealing at 550 °C for 10 h. (c) Comparison of I-PtNiCo-NW/C-15 nm and I-PtCo-NW/C. (d) PtNiCo-NW/C-5nm before and after thermal annealing at 550 °C for 10 and 20 h, respectively.

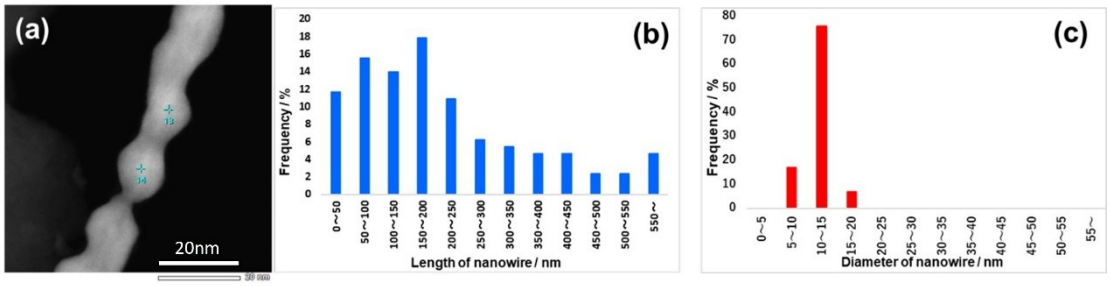

Figure S7. (a) STEM image, (b) length distribution and (c) diameter distribution of D-PtNiCo-NW/C-15 nm.

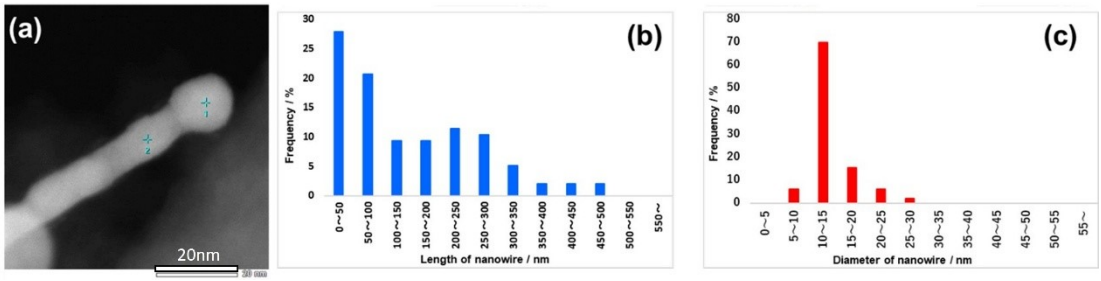

Figure S8. (a) STEM image, (b) length distribution and (c) diameter distribution of I-PtNiCo-NW/C-15 nm.

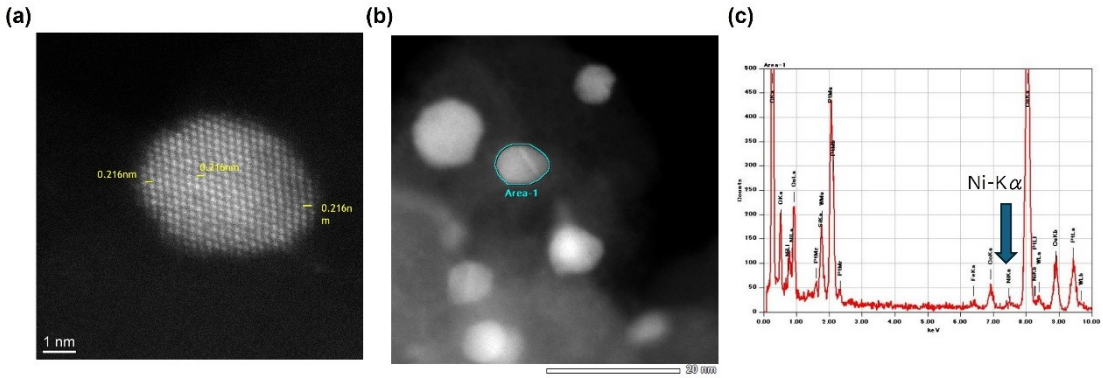

Figure S9 (a) High resolution HAADF-STEM image of <5 nm sample after 20 h annealing. (b) HAADF-STEM image of a representative region in the <5 nm sample after 20 h annealing and (c) area-selected EDS spectrum of area selected in (b).

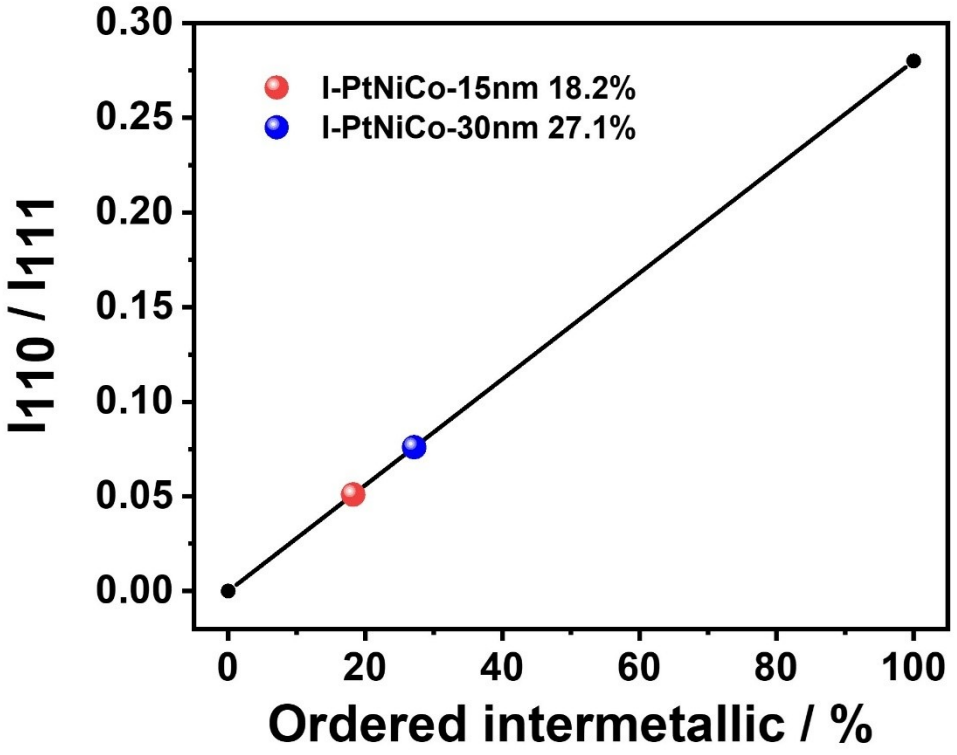

Figure S10 Ordering degree of PtNiCo-NWs catalysts with different diameters.

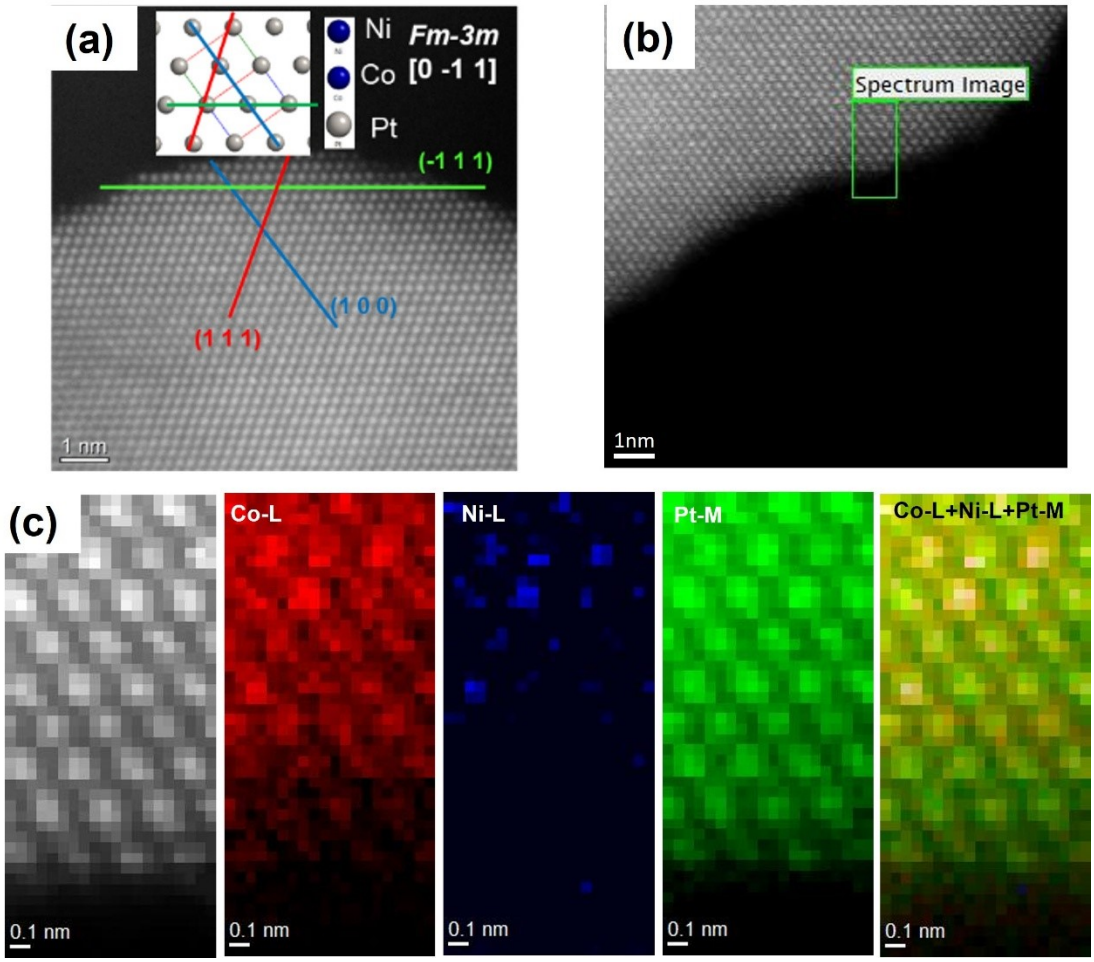

Figure S11. (a,b) HAADF-STEM image and (c) STEM-EELS mappings for D-PtNiCo-NW/C-15 nm.

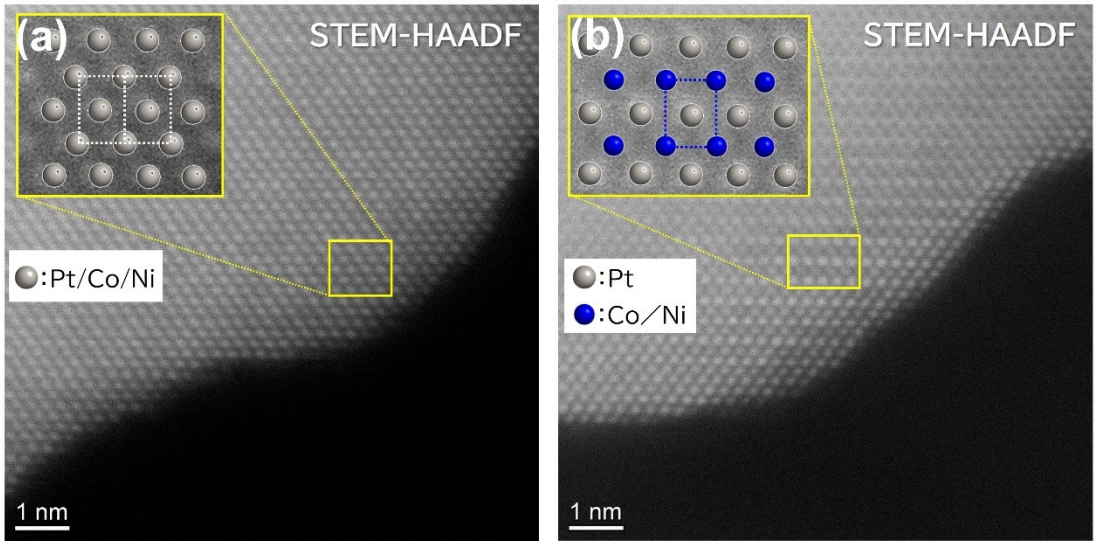

Figure S12. (a) HAADF-STEM image of D-PtNiCo-NW/C-15 nm showing atomic arrangement. (b) HAADF-STEM image of I-PtNiCo-NW/C-15 nm showing atomic arrangement.

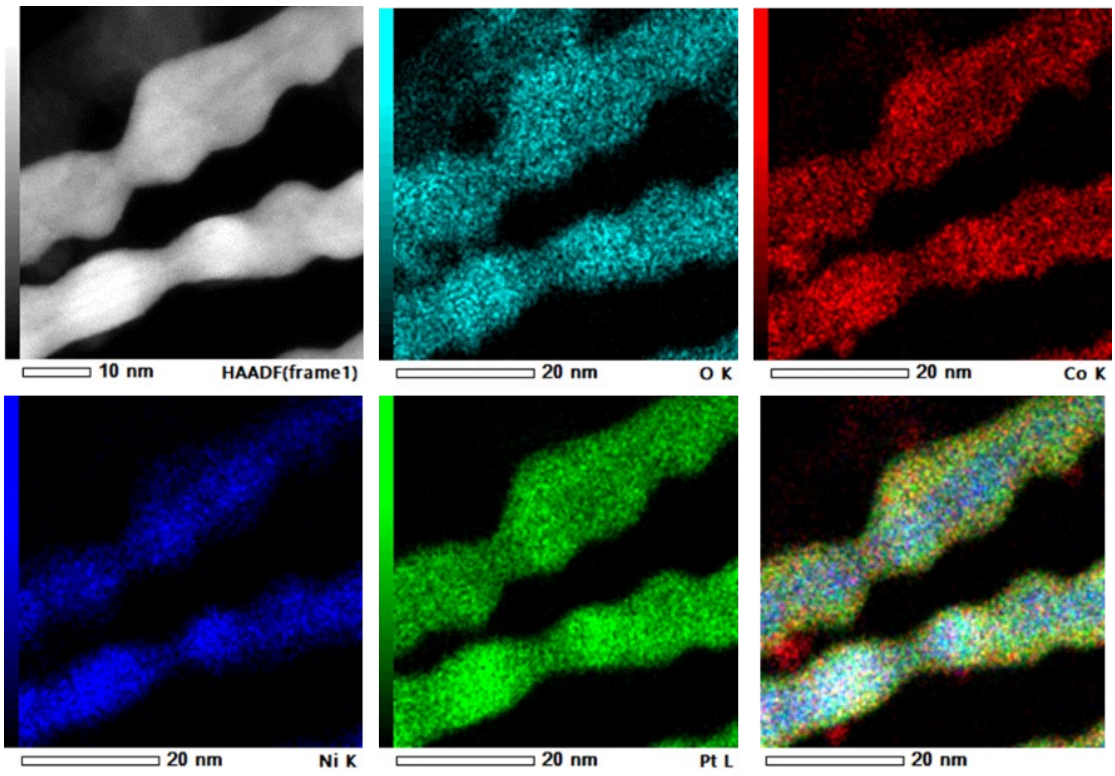

Figure S13. STEM-EDS element mapping spectrum of D-PtNiCo-NW/C-15 nm.

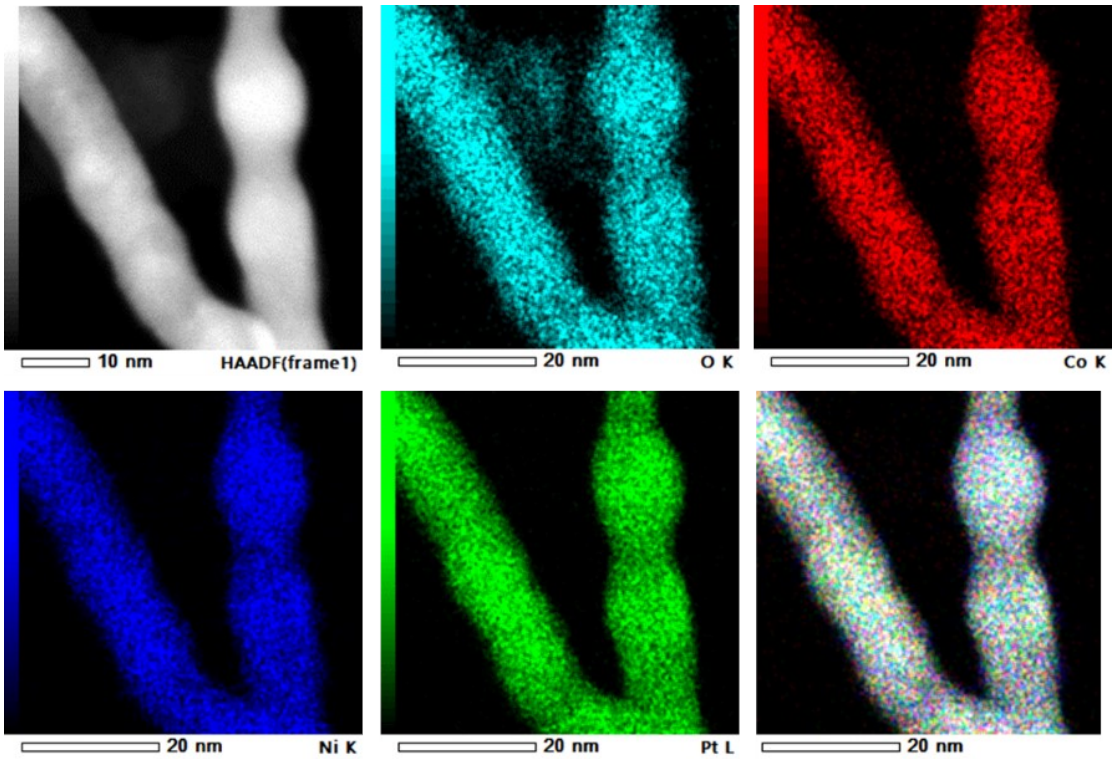

Figure S14. STEM-EDS element mapping spectrum of I-PtNiCo-NW/C-15 nm

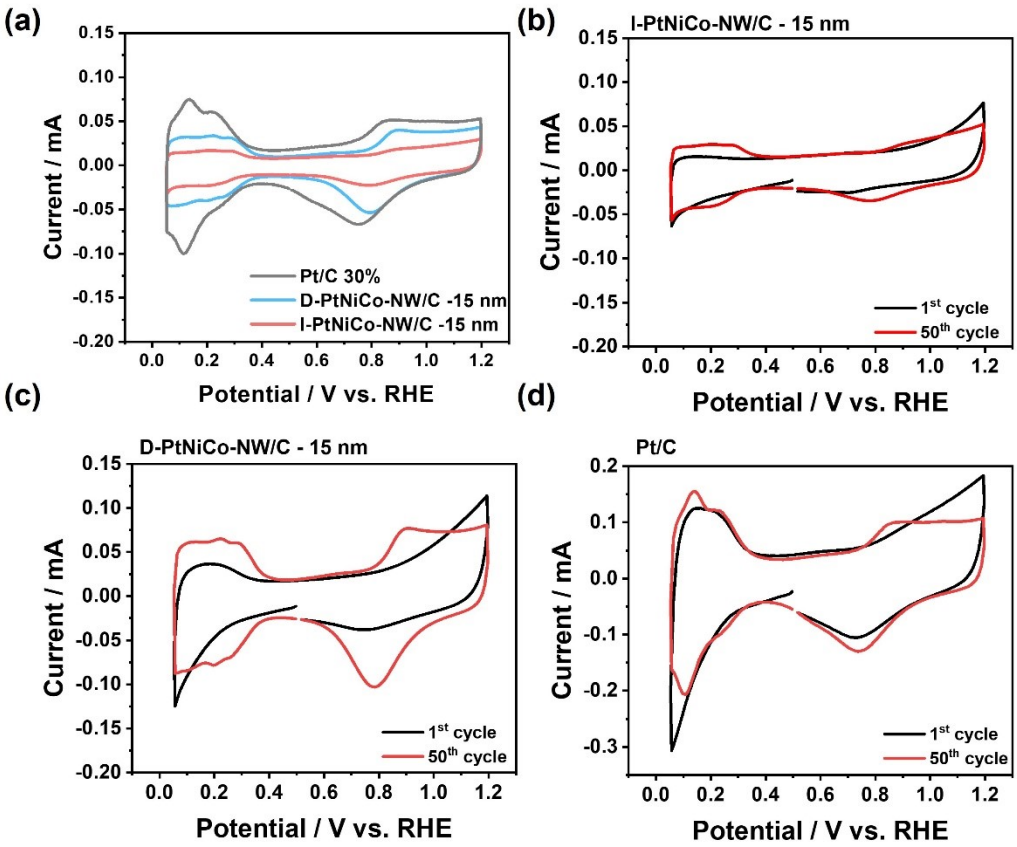

Figure S15 (a) Comparison of CV curves of ordered and disordered PtNiCo-NW/C -15 nm with commercial Pt/C 30% catalysts as reference at a scanning rate 50 mV/s. CV curves of the first cycle and the 50th cycle of (b) I-PtNiCo-NW/C -15 nm, (c) D-PtNiCo-NW/C -15 nm, and (d) Pt/C 30% at a scanning rate of 100 mV/s.

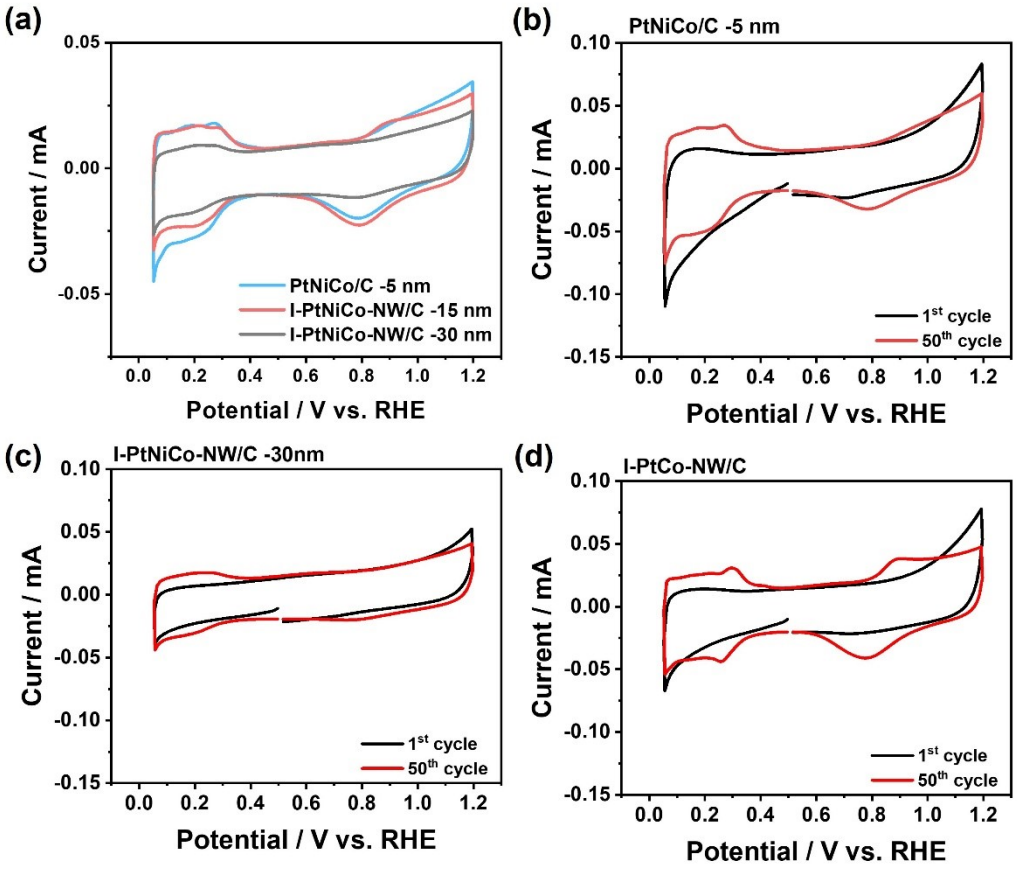

Figure S16 (a) Comparison of CV curves of PtNiCo-NW/C with different diameters after heat treatment at 550°C for 10h at a scanning rate 50 mV/s. CV curves of first cycle and the 50th cycle of (b) PtNiCo-NW/C -5 nm, (c) I-PtNiCo-NW/C -30 nm and (d) I-PtCo-NW/C at a scanning rate for 100 mV/s.

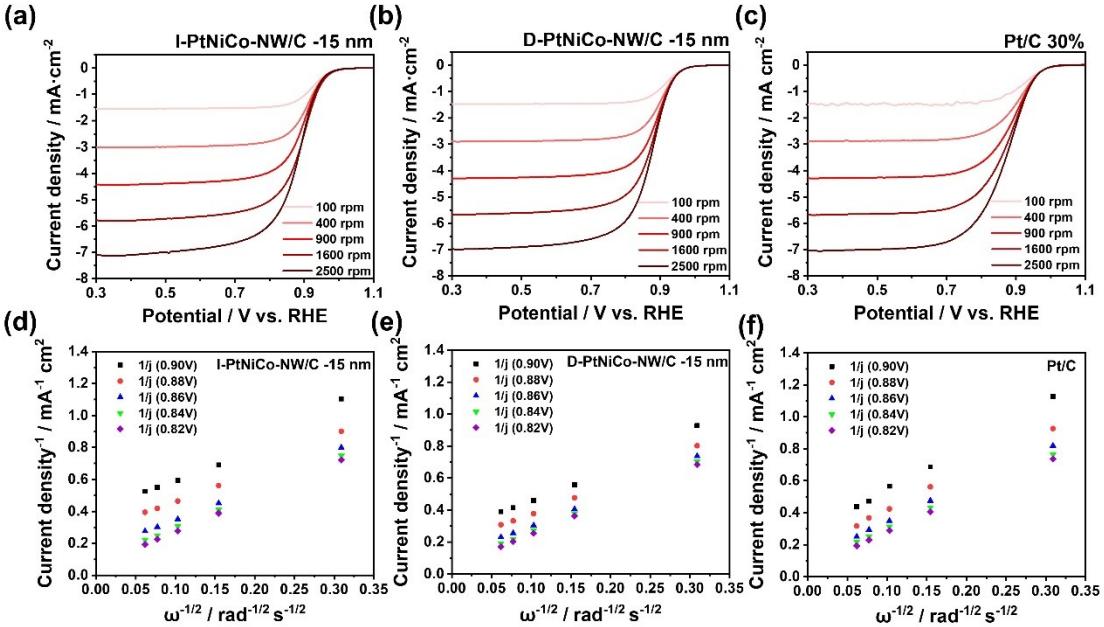

Figure S17 LSV curves and Koutecky-Levich plots for (a, d) I-PtNiCo-NW/C -15 nm, (b, e) D-PtNiCo-NW/C -15 nm, and (c,f) Pt/C 30% in O_2-saturated 0.1 M $HClO_4$ solution at different rotating speed.

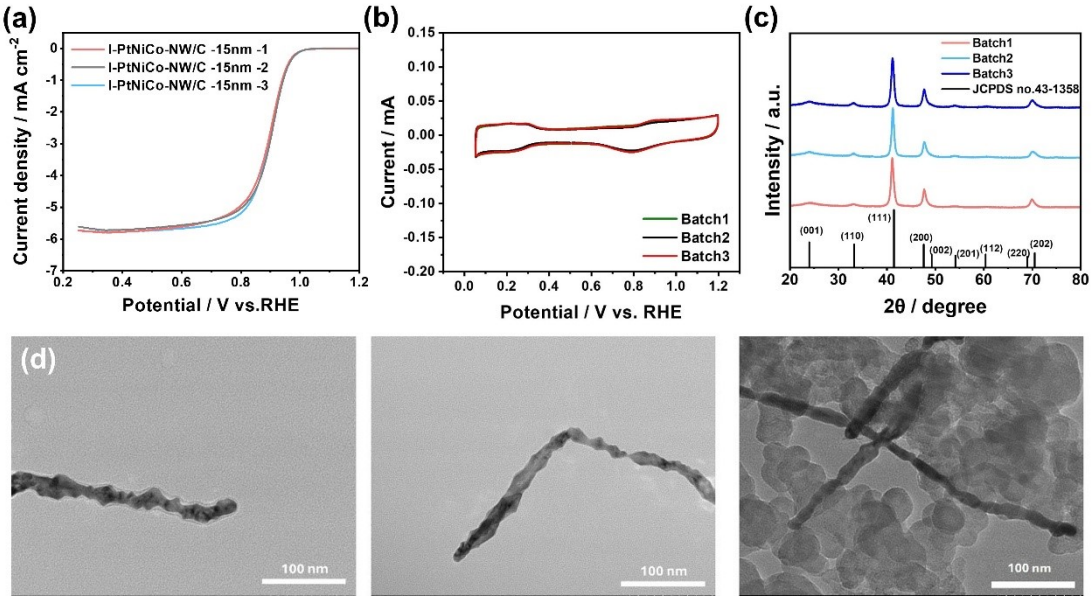

Figure S18 Reproducibility of 3 batches of I-PtNiCo-NW/C -15 nm checked by (a) LSV curves, (b) CV curves, (c) XRD patterns and (d) TEM images.

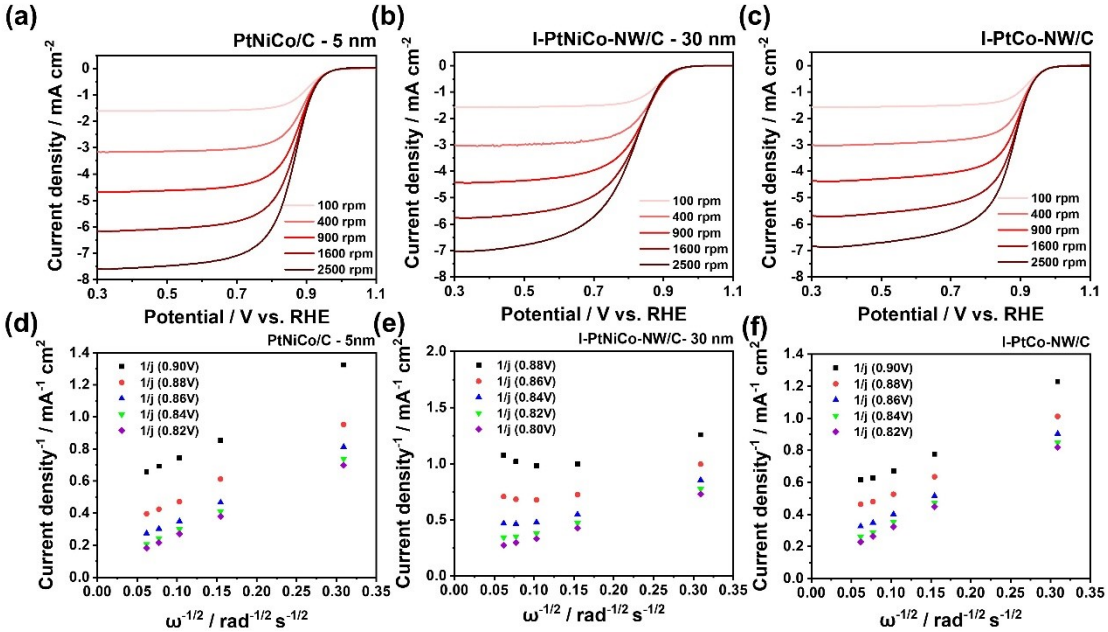

Figure S19 LSV curves and Koutecky-Levich plots for (a, d) PtNiCo-NW/C -5 nm, (b, e) I-PtNiCo-NW/C -30 nm, and (c,f) I-PtCo-NW/C in O_2-saturated 0.1 M $HClO_4$ solution at different rotating speed.

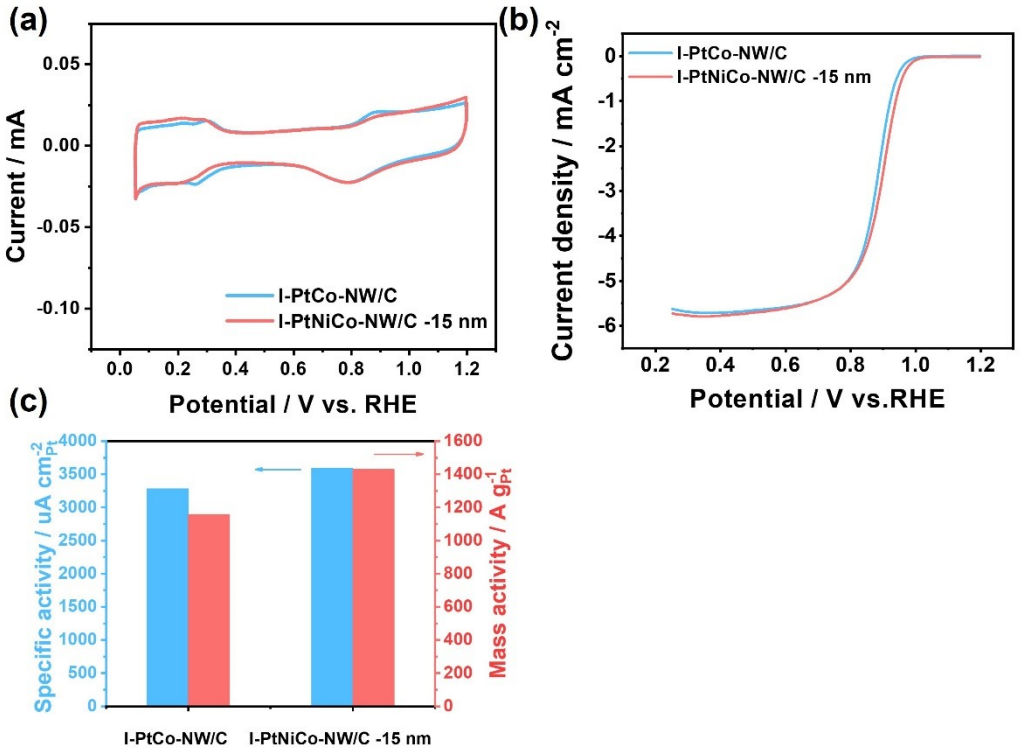

Figure S20 (a) CV at a scanning rate 50 mV/s, (b) LSV curves and (c) comparison of mass (blue) and specific (red) activity of I-PtNiCo-NW/C-15 nm and I-PtCo-NW/C.

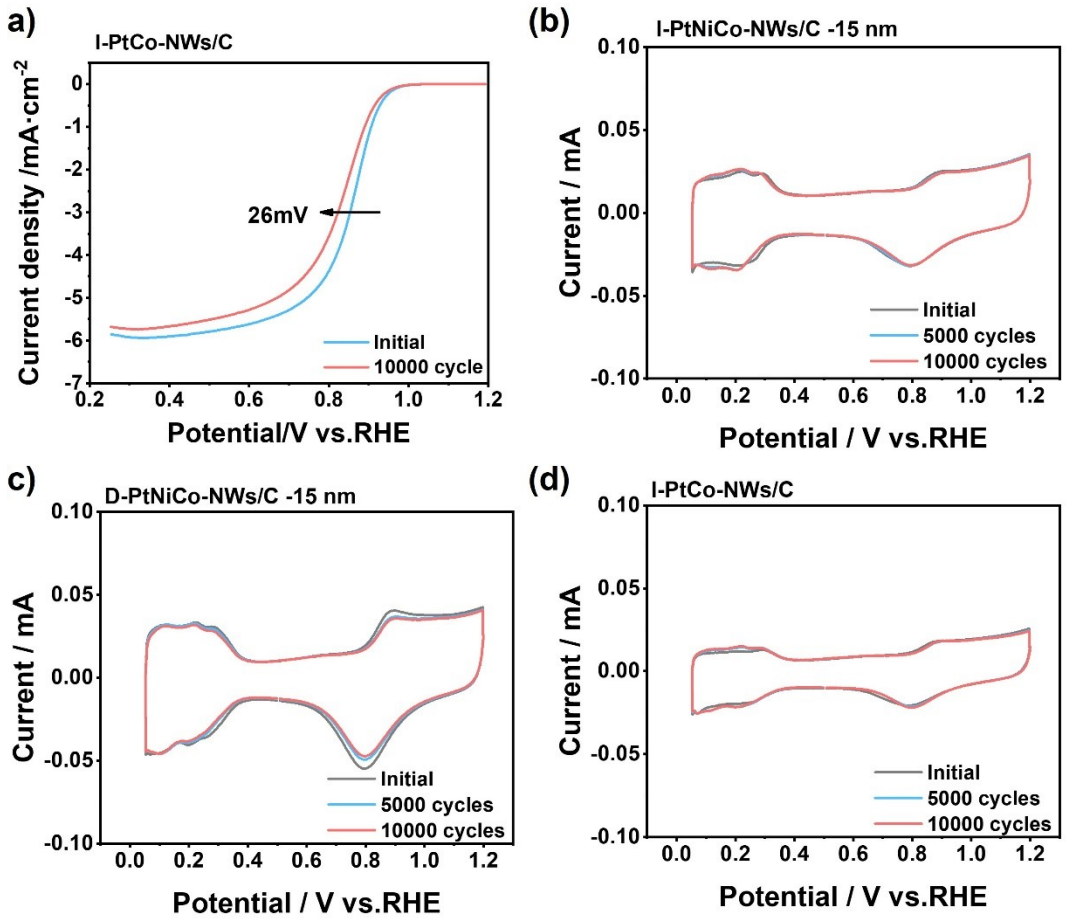

Figure S21 (a) ORR polarization curves of I-PtCo-NW/C before and after the ADT. CV curves of Initial cycle, after 5000 ADT cycles and 10000 cycles of (b) I-PtNiCo-NW/C-15 nm, (c) D-PtNiCo-NW/C-15 nm and (d) I-PtCo-NW/C at a scanning rate 50 mV/s**.**

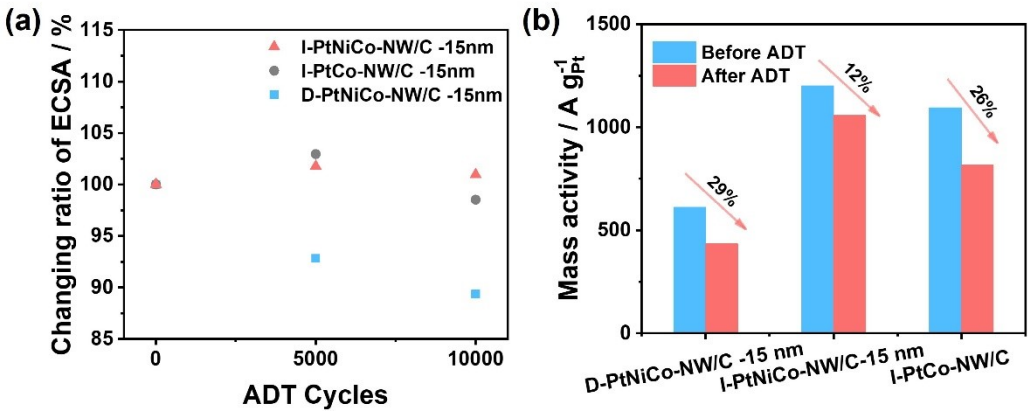

Figure S22 (a) ECSA changing ratio of the I-PtNiCo-NW/C-15 nm, D-PtNiCo-NW/C-15 nm and I-PtCo-NW/C during the ADT cycles in the RDE test. (b) Mass activity changes before and after the ADT cycles of the catalysts.

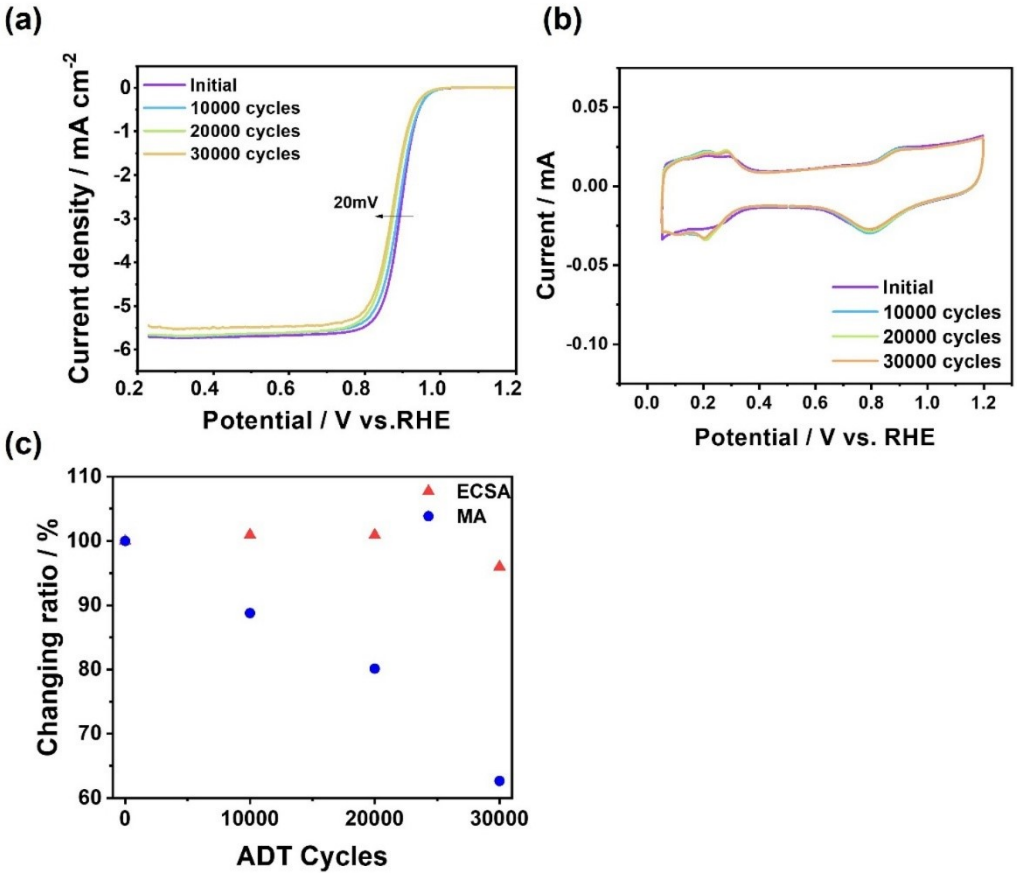

Figure S23 (a) ORR polarization curves and (b) CV curves of I-PtNiCo-NW/C-15 nm before and after the ADT for 30 k cycles. (c) ECSA and MA changing ratio before and after the ADT cycles of the catalysts.

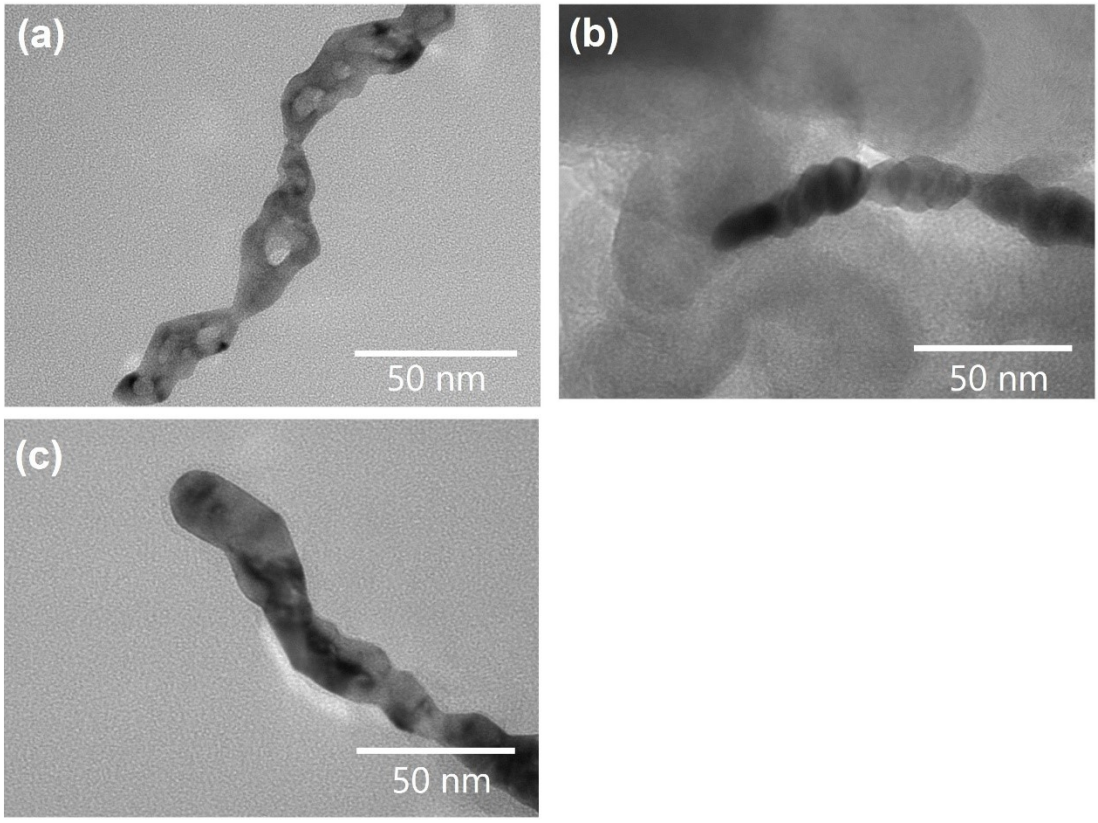

Figure S24. TEM images of (a) D-PtNiCo-NW/C-15 nm, (b) I-PtNiCo-NW/C-15 nm and (c) I-PtCo-NW/C catalyst after 10K ADT cycles.

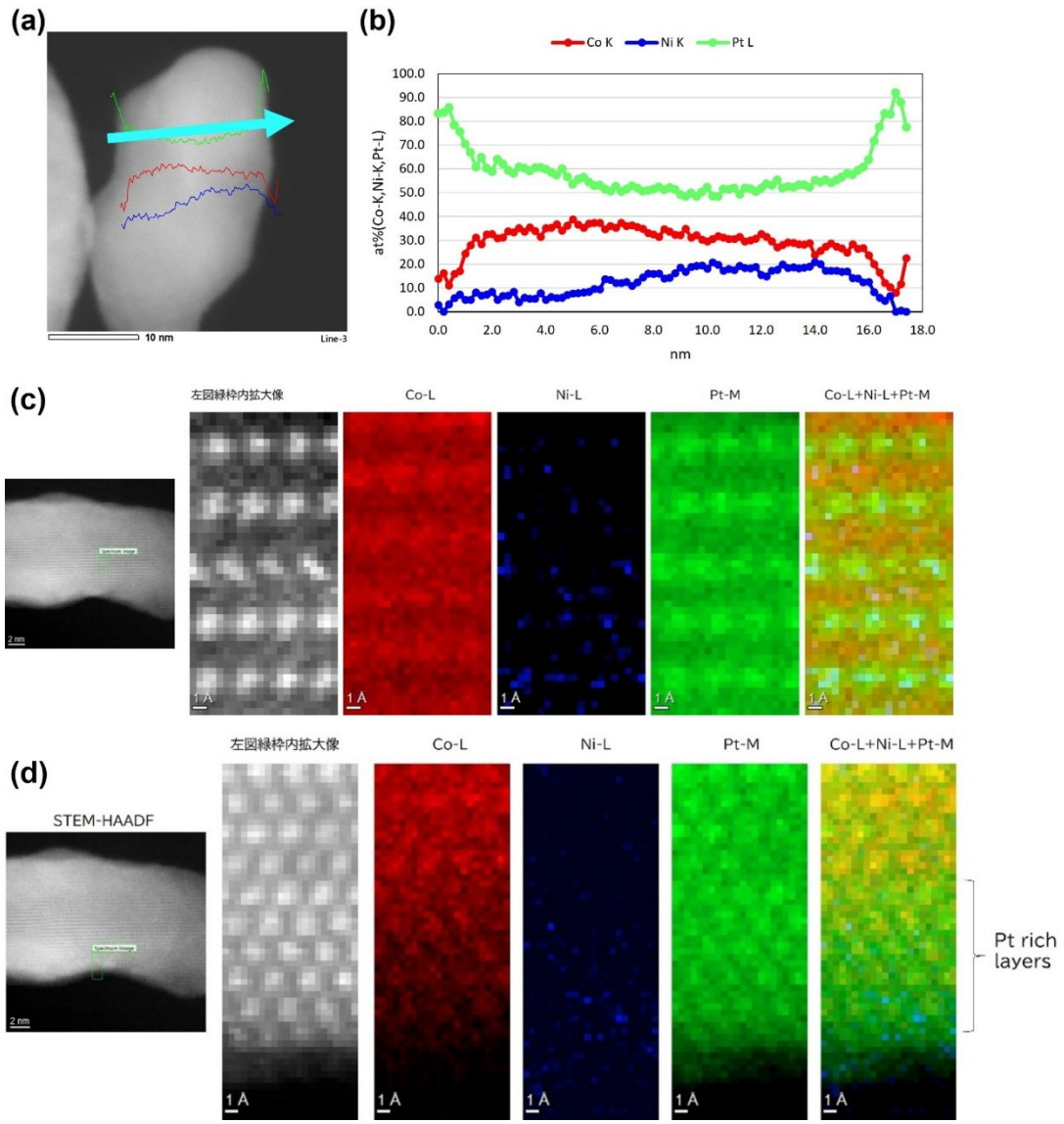

Figure S25 (a,b) STEM-EDX line scans for I-PtNiCo-NW/C-15 nm-after. STEM-EELS mappings for I-PtNiCo-NW/C-15 nm-after ADT of (c) outer and (d) inner area of NWs

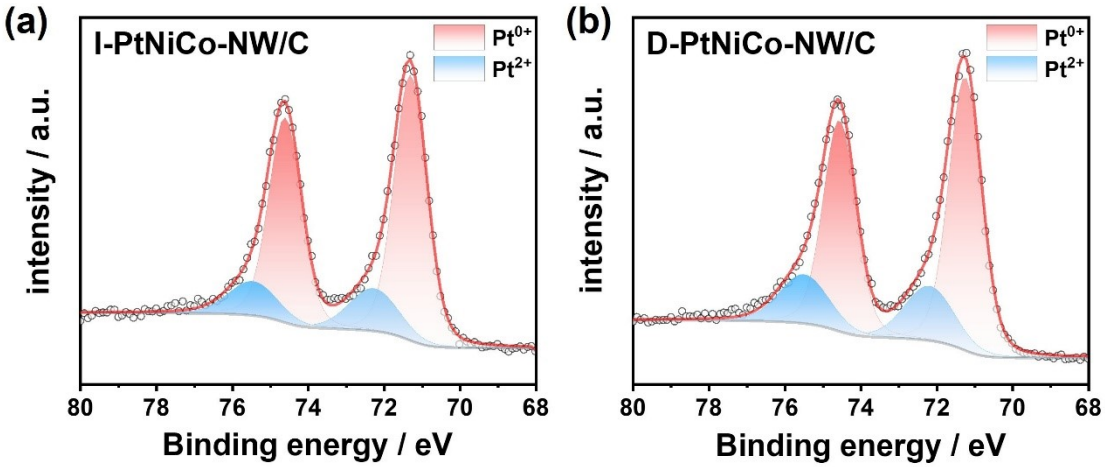

Figure S26. XPS spectra with peaks fitting of Pt 4f for (a) I-PtNiCo-NW/C-15 nm and (b) D-PtNiCo-NW/C-15 nm.

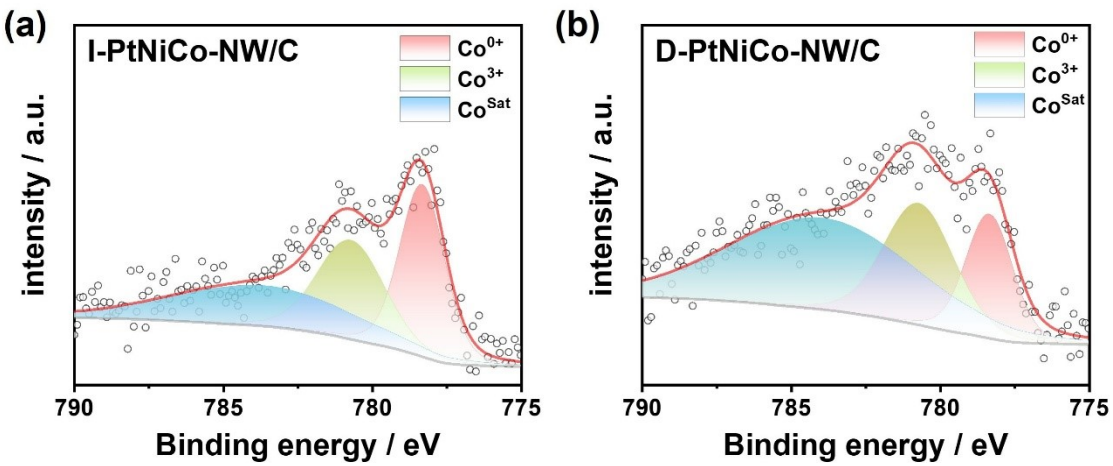

Figure S27. XPS spectra with peaks fitting of Co $2p_{2/3}$ for (a) I-PtNiCo-NW/C-15 nm and (b) D-PtNiCo-NW/C-15 nm

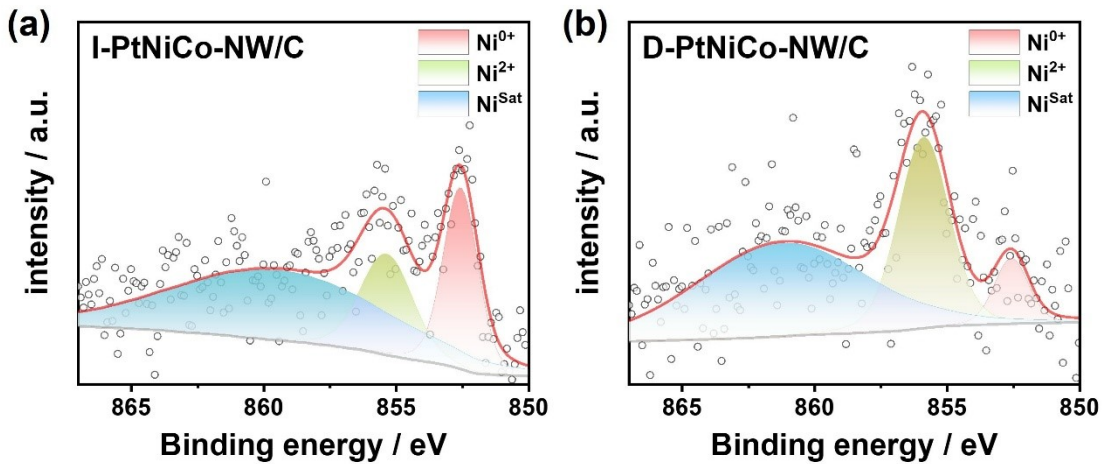

Figure S28. XPS spectra with peaks fitting of Ni $2p_{2/3}$ for (a) I-PtNiCo-NW/C-15 nm and (b) D-PtNiCo-NW/C-15 nm

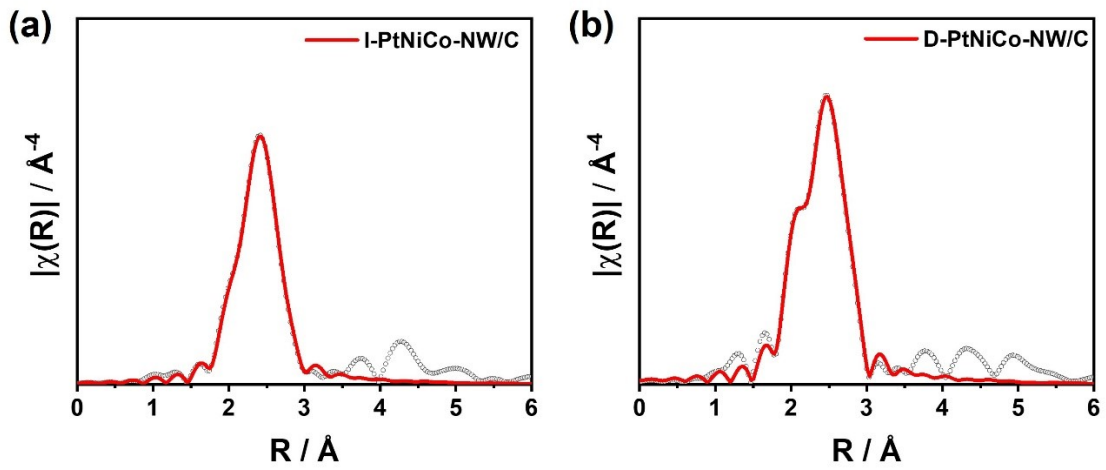

Figure S29. Pt L_3-edge FT-EXAFS spectra and the fitting results of (a) I-PtNiCo-NW/C-15 nm and (b) D-PtNiCo-NW/C-15 nm.

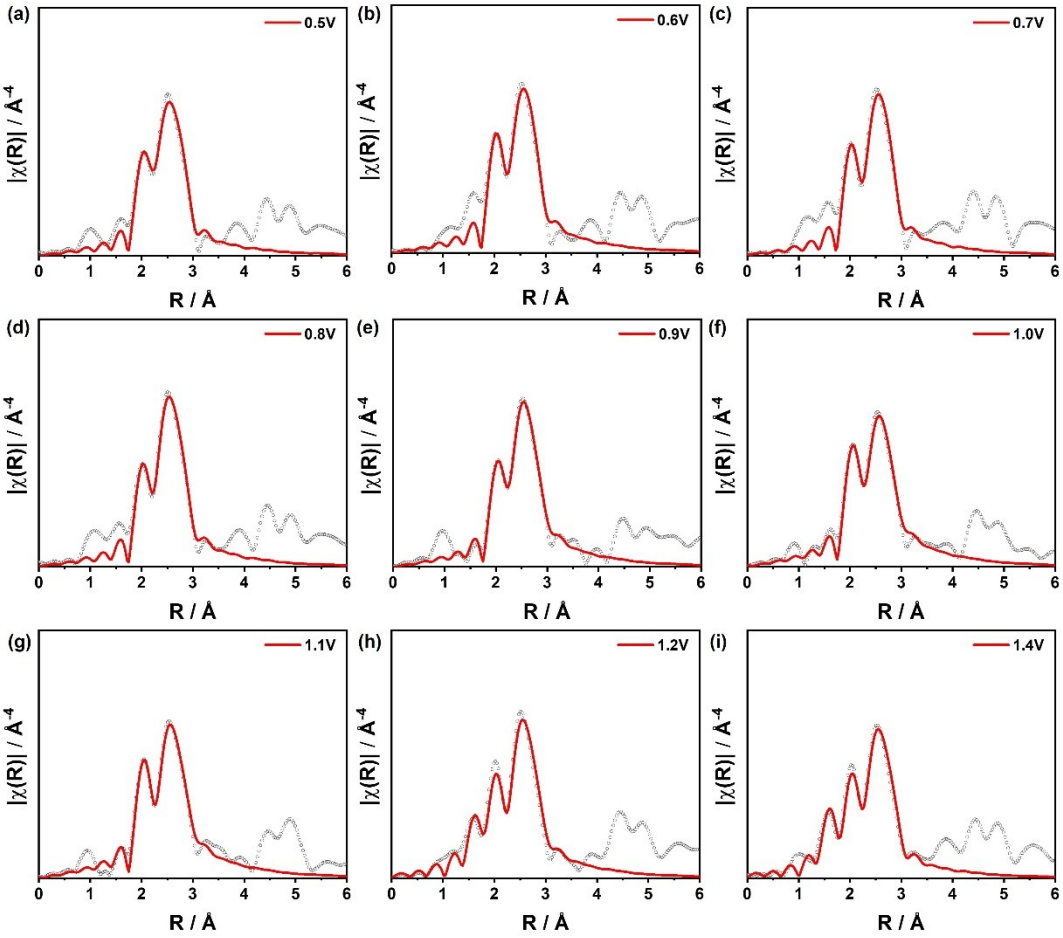

Figure S30. Pt L3-edge FT-EXAFS spectra and corresponding fittings for D-PtNiCo-NW/C-15 nm at (a) 0.5 V, (b) 0.6 V, (c) 0.7 V, (d) 0.8 V, (e) 0.9 V, (f) 1.0 V, (g) 1.1 V, (h) 1.2 V and (i) 1.4 V.

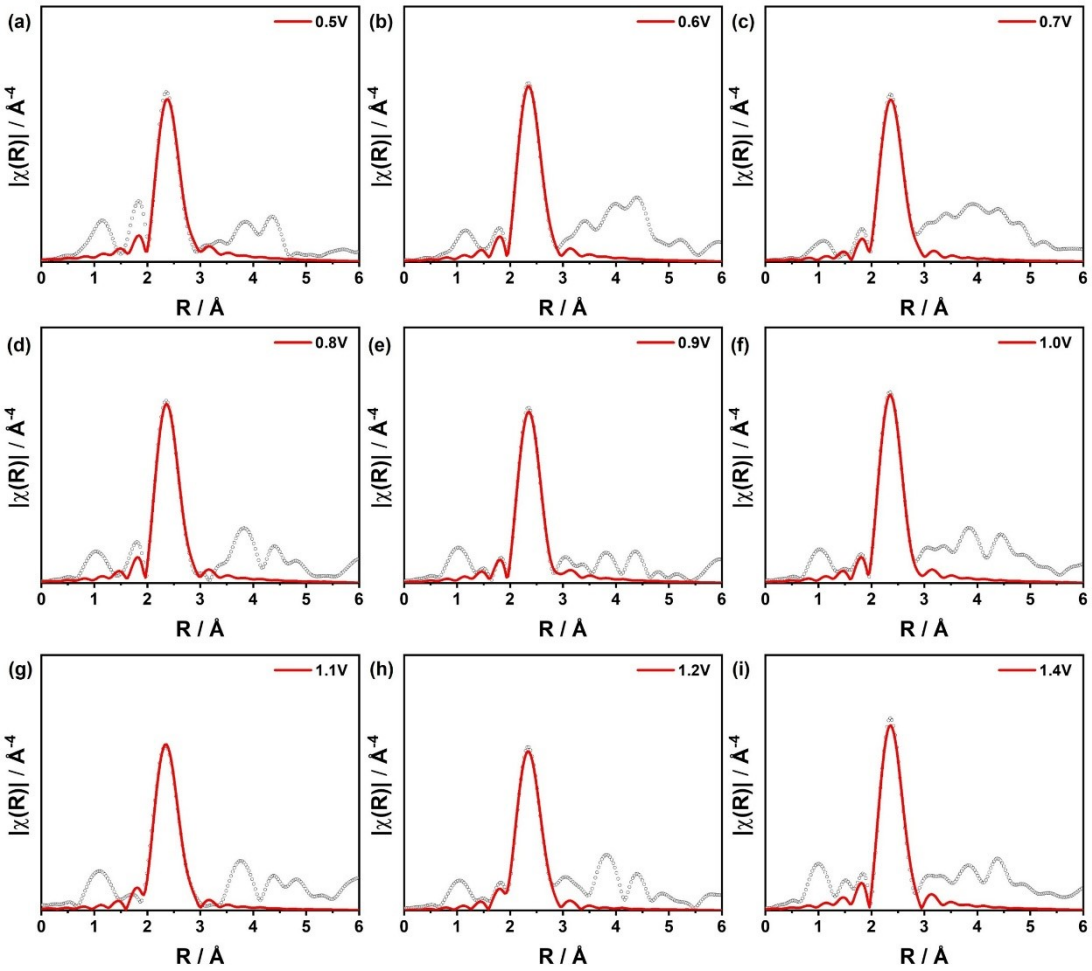

Figure S31. Pt L3-edge FT-EXAFS spectra and corresponding fittings for I-PtNiCo-NW/C-15 nm at (a) 0.5 V, (b) 0.6 V, (c) 0.7 V, (d) 0.8 V, (e) 0.9 V, (f) 1.0 V, (g) 1.1 V, (h) 1.2 V and (i) 1.4 V.

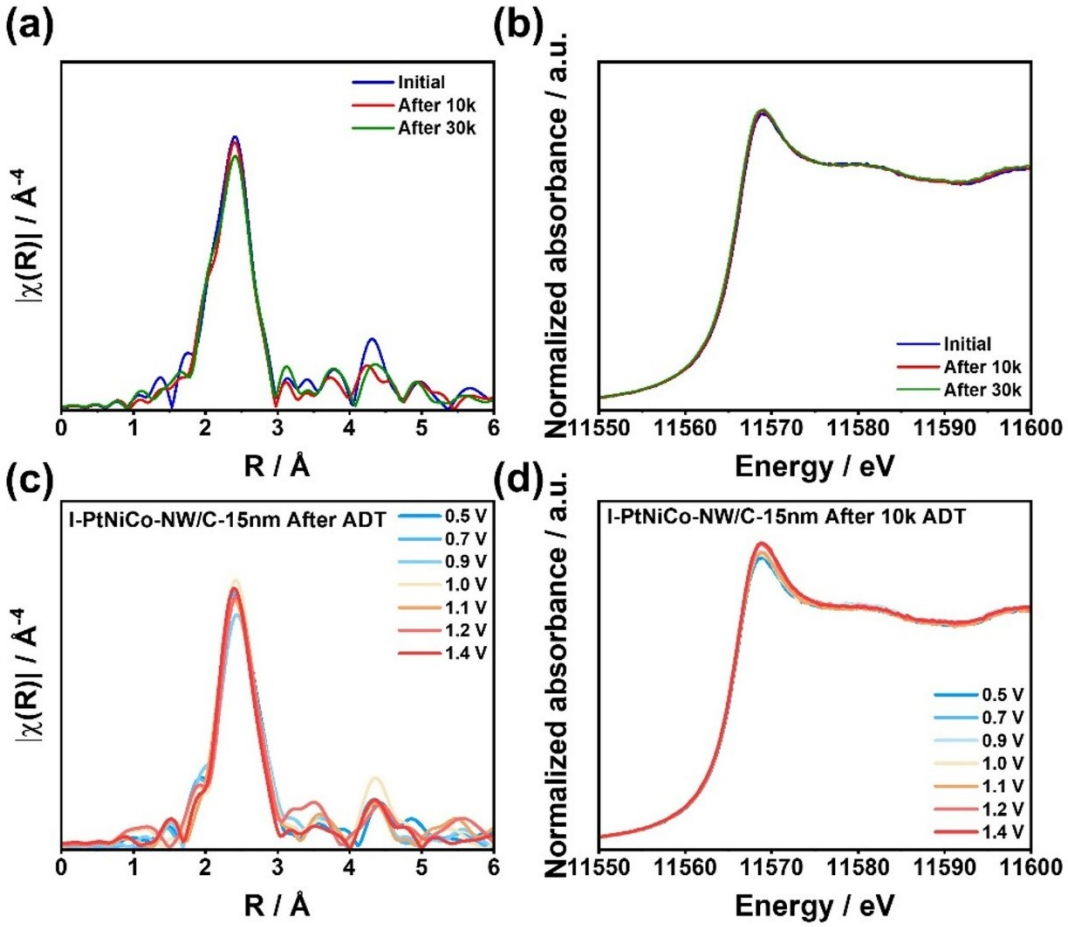

Figure S32 Ex situ Pt L_3-edge (a) FT-EXAFS and (b) XANES spectra for I-PtNiCo-NW/C-15 nm Before and after ADT. *Operando* Pt L_3-edge (c) FT-EXAFS and (d) XANES spectra for I-PtNiCo-NW/C-15 nm After ADT

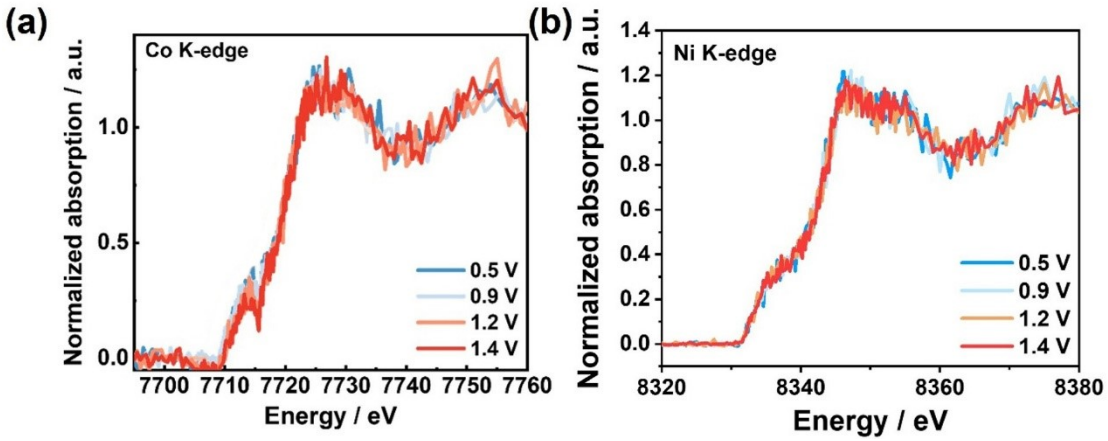

Figure S33. *operando* HERFD- (a) Co K-edge and (b) Ni K-edge XANES analysis for I-PtNiCo-NW/C-15 nm.

Table S1 ICP results of PtNiCo NWs at different heating ramp

Heating ramp	Pt (at%)	Co(at%)	Ni(at%)
Direct (15 nm)	50	36	14
6^{o}C /min	50	34	16
3^{o}C/min (30 nm)	49	34	17

Table S2 A summary of lattice parameters of different nanowire samples.

Catalyst	**2theta / degree (111)**	**Crystalline size nm**	**Interplanar spacing nm**
I-PtNiCo-15nm	41.2495	2.387976	0.2186824
D-PtNiCo-15nm	41.01326	1.049868	0.2198873
I-PtNiCo-5nm	40.7737	1.359715	0.2211238
I-PtNiCo-30nm	41.50562	2.456332	0.217392
I-PtCo	40.87608	3.604799	0.2205935

Table S3 Strain effect of I-PtNiCo-NW/C-15 nm comparing to D-PtNiCo-NW/C-15 nm and I-PtCo-NW/C.

I-PtNiCo-15nm comparing with:	Strain %
D-PtNiCo-15nm	0.548
I-PtCo	0.866

Table S4. Comparison of ORR performance for I-PtNiCo-NW/C-15 nm with other reported Pt-based electrocatalysts.

Catalyst	Mass activity at 0.9 V (A mg_{Pt}^{-1})	Specific activity at 0.9 V (mA cm_{Pt}^{-2})	Degradation of half wave potential after ADT test		Ref
			Loss(mV)	Cycles	
PtNi-NW/C	1.37	2.07	6.2	10k	[1]
PtNiMo-NW/C	2.89	3.13	<1	80k	[2]
g-Co–N–C/PtCo	1.67	3.08	4	10k	[3]
g-Ni–N–C/PtCo	1.62	3.01	0	10k	
IMC-PtFeMo/C nanowire	2.56	5.41	2	10k	[4]
PtCo-IW/KJ300	1.54	3.0	NA	NA	[5]
A1-Pt_3Co/C nanowire	0.12	1.1	9	5k	[6]
$L1_2$-Pt_3Co/C nanowire	0.31	2.47	0	5k	
fct-PtFeIr/C	2.03	2.40	~0	10k	[7]
MSA-PtCo/C	0.65	0.91	NA	NA	[8]
$NW_{493\ K}$/C	0.28	0.39	~0	2k	[9]
o-Pt_2NiCo	0.44	1.37	14	30k	[10]
I-PtNiCo-NW/C-15 nm	1.43	3.59	5	10k	**This work**

Table S5. The deconvolution result of Pt 4f XPS spectra.

Sample	Pt^{0+} (%) (Right +Left peak)	Pt^{2+} (%) (Right +Left peak)
D-PtNiCo-NW/C-15 nm	42.70+33.02=75.72	12.78+11.50=24.28
I- PtNiCo-NW/C-15 nm	45.31+34.98=80.29	10.93+8.77=19.7

Table S6. The deconvolution result of Ni $2p_{2/3}$ XPS spectra.

Sample	Ni^{0+} (%)	Ni^{2+} (%)	Ni^{sat} (%)
D-PtNiCo-NW/C-15 nm	7.99	35.03	56.98
I- PtNiCo-NW/C-15 nm	23.62	19.80	56.59

Table S7. The deconvolution result of Co $2p_{2/3}$ XPS spectra.

Sample	Co^{0+} (%)	Co^{3+} (%)	Co^{sat} (%)
D-PtNiCo-NW/C-15 nm	18.48	27.16	54.36
I- PtNiCo-NW/C-15 nm	35.40	30.58	34.02

Table S8. The corresponding R space curve fitting results of Pt L_3-edge for the samples compared with Pt foil standard.

Sample	Shell	CN	R (Å)	σ^2 ($Å^2$)	ΔE_0(eV)	R factor
Pt foil	Pt-Pt	12	2.764± 0.001	0.005	7.2	0.001
D-PtNiCo-NW/C-15 nm	Pt-Pt	6.0±0.9	2.705± 0.004	0.006	6.1	0.004
	Pt-Co/Ni	3.8±0.7	2.629± 0.009	0.008		
I-PtNiCo-NW/C-15 nm	Pt-Pt	5.2±0.6	2.688± 0.002	0.005	7.0	0.001
	Pt-Co/Ni	5.7±0.4	2.628± 0.003	0.006		

(a) CN, coordination number; (b) R, distance between absorber and backscatter atoms; (c) σ^2, Debye-Waller factor to account for both thermal and structural disorders; (d)ΔE_0, inner potential correction; R factor indicates the goodness of the fit. $S0^2$ was fixed to 0.863, according to the experimental EXAFS fit of Pt foil by fixing CN as the known crystallographic value. Fits were undergone in R-space for 1.8≤R≤3.1 Å, and the $k^{1,2,3}$ weighting for $\Delta k = 3 – 14$ $Å^{-1}$. The distance of the Pt-Pt and Pt-Co are from the crystal structure of PtCo-intermetallic phase (P4-mmm) for ordered structure and PtCo-A alloy phase (fm-3m) for disordered phase.

Table S9 The corresponding R space curve fitting results of Pt L_3-edge for the D-PtNiCo-NW/C-15 nm catalysts varying different potential.

Potential	Shell	CN[a]	R (Å)[b]	σ^2(Å^2)[c]	ΔE_0 (eV)[d]	R factor
0.5 V	Pt-Pt	6.2±0.6	2.714±0.015	0.004	4.5	0.011
	Pt-Co/Ni	3.1±0.9	2.601±0.021	0.007		
0.6 V	Pt-Pt	5.2±0.6	2.709±0.008	0.003	4.0	0.014
	Pt-Co/Ni	3.6±0.6	2.593±0.022	0.006		
0.7 V	Pt-Pt	6.2±0.3	2.710±0.005	0.004	2.7	0.014
	Pt-Co/Ni	3.8±0.2	2.594±0.026	0.009		
0.8 V	Pt-Pt	5.6±0.4	2.713±0.002	0.003	4.9	0.006
	Pt-Co/Ni	3.9±0.8	2.610±0.015	0.009		
0.9 V	Pt-Pt	3.3±0.2	2.714±0.011	0.001	5.1	0.003
	Pt-Co/Ni	4.2±0.1	2.611±0.012	0.007		
1.0 V	Pt-Pt	2.9±0.4	2.715±0.007	0.001	3.3	0.006
	Pt-Co/Ni	3.7±0.7	2.595±0.011	0.005		
1.1 V	Pt-Pt	2.9±0.9	2.716±0.008	0.001	4.6	0.008
	Pt-Co/Ni	3.4±0.2	2.601±0.009	0.006		
1.2 V	Pt-Pt	3.5±0.6	2.720±0.005	0.002	6.3	0.019
	Pt-Co/Ni	3.1±0.1	2.615±0.010	0.006		
	Pt-O	2.1±0.5	2.121±0.003	0.001	-18.3	
1.4 V	Pt-Pt	4.7±1.3	2.724±0.011	0.001	7.9	0.008
	Pt-Co/Ni	3.0±0.4	2.616±0.012	0.009		
	Pt-O	2.2±0.4	2.111±0.005	0.001	-24.2	

(a) CN, coordination number; (b) R, distance between absorber and backscatter atoms; (c) σ^2, Debye-Waller factor to account for both thermal and structural disorders; (d) ΔE_0, inner potential correction; R factor indicates the goodness of the fit. $S0^2$ was

fixed to 0.863, according to the experimental EXAFS fit of Pt foil by fixing CN as the known crystallographic value. Fits were undergone in R-space for 1.8≤R≤3.1 Å, and the k [1,2,3] weighting for Δk = 3 – 13 $Å^{-1}$. The distance of the Pt-Pt and Pt-Co are from the crystal structure of PtCo-intermetallic phase (P4-mmm) for ordered structure and PtCo-A alloy phase (fm-3m) for disordered phase.

Table S10 The corresponding R space curve fitting results of Pt L_3-edge for the I-PtNiCo-NW/C-15 nm catalysts varying different potential.

Potential	Shell	CN[a]	R (Å)[b]	σ^2(Å^2)[c]	ΔE_0 (eV)[d]	R factor
0.5 V	Pt-Pt	6.8±0.8	2.690±0.008	0.010	11.1	0.010
	Pt-Co/Ni	3.1±0.6	2.659±0.011	0.001		
0.6 V	Pt-Pt	6.2±0.4	2.694±0.009	0.009	8.2	0.007
	Pt-Co/Ni	4.1±0.4	2.645±0.013	0.002		
0.7 V	Pt-Pt	6.3±0.3	2.693±0.004	0.009	9.3	0.030
	Pt-Co/Ni	4.8±0.6	2.657±0.008	0.003		
0.8 V	Pt-Pt	6.5±0.9	2.696±0.012	0.009	9.6	0.007
	Pt-Co/Ni	4.3±0.4	2.651±0.006	0.002		
0.9 V	Pt-Pt	6.8±0.2	2.698±0.006	0.011	8.3	0.011
	Pt-Co/Ni	4.2±0.3	2.656±0.005	0.002		
1.0 V	Pt-Pt	6.5±0.6	2.700±0.012	0.011	6.1	0.020
	Pt-Co/Ni	4.0±0.2	2.645±0.011	0.003		
1.1 V	Pt-Pt	6.2±0.5	2.706±0.013	0.005	6.8	0.004
	Pt-Co/Ni	3.8±0.5	2.637±0.007	0.002		
1.2 V	Pt-Pt	6.0±0.8	2.712±0.003	0.006	6.4	0.020
	Pt-Co/Ni	3.5±0.6	2.626±0.007	0.002		
1.4 V	Pt-Pt	5.8±0.5	2.718±0.009	0.010	8.6	0.018
	Pt-Co/Ni	3.0±0.3	2.643±0.006	0.001		

(a) CN, coordination number; (b) R, distance between absorber and backscatter atoms; (c) σ^2, Debye-Waller factor to account for both thermal and structural disorders; (d) ΔE_0, inner potential correction; R factor indicates the goodness of the fit. $S0^2$ was fixed to 0.863, according to the experimental EXAFS fit of Pt foil by fixing CN as the known crystallographic value. Fits were undergone in R-space for 1.8≤R≤3.1 Å, and the k [1,2,3] weighting for Δk = 3 – 13 Å^{-1}. The distance of the Pt-Pt and Pt-Co are from

the crystal structure of PtCo-intermetallic phase (P4-mmm) for ordered structure and PtCo-A alloy phase (fm-3m) for disordered phase.

Reference

1. W. Cao, N. Thakur, M. Kumar, T. Uchiyama, Y. Gao, S. Tominaka, A. Machida, T. Watanabe, R. Sato, T. Teranishi, M. Matsumoto, H. Imai, Y. Sakurai and Y. Uchimoto, *J. Mater. Chem. A*, 2024, **12**, 29843-29853.
2. L. Gao, T. Sun, X. Chen, Z. Yang, M. Li, W. Lai, W. Zhang, Q. Yuan and H. Huang, *Nat Commun*, 2024, **15**, 508.
3. Z. Huang, Y. Wang, J. Xia, S. Hu, N. Chen, T. Ding, C. Zhan, C. W. Pao, Z. Hu, W. H. Huang, T. Shi, X. Meng, Y. Xu, L. Cao and X. Huang, *Sci. Adv.*, 2024, **10**.
4. C. Li, D. Liu, P. Qin, G. Peng, J. Shui, L. Shang and T. Zhang, *Nano Energy*, 2024, **129**.
5. X. Niu, R.-Y. Shao, L. Zhang, C. Xu, T.-W. Song, P. Yin, L. Tong, C. Su and H.-W. Liang, *Mater. Chem. Front.*, 2023, **7**, 3390-3397.
6. Y. Su, Z. Wang, R. Gao, Q. Wu, J. Zhao, G. Zhu, Q. Li, H. Xu, Y. Pan, K. Gu, C. Biz, M. Fianchini and J. Gracia, *Adv. Funct. Mater.*, 2023, **34**.
7. Z. Yang, H. Yang, L. Shang and T. Zhang, *Angew. Chem. Int. Ed. Engl.* 2022, **61**, e202113278.
8. L. Zhang, L. Tong, S. Li, C.-S. Ma, K.-Z. Xue and H.-W. Liang, *J. Energy Chem.*, 2025, **101**, 1-6.
9. Y. Zhuang, Y. Iguchi, T. Li, M. Kato, Y. A. Hutapea, A. Hayashi, T. Watanabe and I. Yagi, *ACS Catal.*, 2024, **14**, 1750-1758.
10. C. Zhang, H. Hu, J. Yang, Q. Zhang, C. Yang and D. Wang, *J. Electrochem.*, 2025, **31(4)**, 2411281.